Scientia Iranica, Vol. 6, No. 2, pp 131-142

SCIENTIA
IRANICA

Analysis of Pulsatile Flow Through Stenotic Arteries

G.R. Zendehbudi[1] and M.S. Moayeri*

In this paper, results of numerical solutions to steady and pulsatile flow through axially symmetric stenoses are presented. The analysis is restricted to laminar flow, Newtonian fluid and rigid boundary. Using a non-orthogonal grid, discrete forms of the transformed governing equations are obtained by a control volume formulation, which are then solved for physical velocity components and pressure. To ensure a true periodic solution, calculations are performed over several periods and the results of two successive periods are compared. To validate the numerical results, several test cases, for which either experimental data or analytical solutions are available, are considered. For the pulsatile flow, an experimentally measured physiological waveform, as well as a simple harmonic pulse having the same stroke volume, are used as the forcing function and the results are compared. It is concluded that although the behavior of these flows may be similar at some instances of time, for an accurate analysis of pulsatile flow through stenotic arteries, the actual physiological waveform should be considered as the inflow boundary condition.

INTRODUCTION

Atherosclerosis is a disease of large and medium size arteries in which deposits of cholesterol and lipid substances on the interior wall of the arteries and proliferation of connective tissues cause a local partial reduction in the arterial cross-sectional area (stenosis). Although there remains uncertainty with regard to the exact mechanisms responsible for the initiation of this phenomena, it has been established that development of atherosclerosis, even in the early stages of the disease, is strongly related to the characteristics of the blood flow in the arteries (e.g. [1,2]). This has attracted the interest of many investigators and, therefore, the hemodynamical characteristics of flow through stenoses, aneurysms and other geometries in the arterial system have been continually investigated over the past 30 years.

Although a large number of investigations has led to better understanding of the flow disturbances induced by a stenosis, most of the theoretical and experimental studies have been performed under different simplifying assumptions. Almost all experimental studies have been performed in rigid stenoses. In most of these studies, the flow has been assumed to be steady [3-6]. Experimental studies of pulsatile flow through rigid stenoses have been reported by Young and Tsai [7], Siouffi et al. [8] and Rabinovits et al. [9]. Lieber and Giddens [10] measured the apparent stresses of turbulent pulsatile flow through a rigid stenosis. Measurements of pulsatile flow in a flexible tube, partially occluded by a hollowed rigid cylinder to model a stenosis, have been carried out by Rooz et al. [11].

A number of numerical and approximate analytical studies on the blood flow through stenotic arteries have been presented in the literature. Numerical solutions of steady flow through axially symmetric rigid stenoses, with blood as a Newtonian fluid, have been reported by several investigators, among which are Deshpande et al. [12], Fukushima et al. [13], Lee [14] and Siegel et al. [15]. This problem, taking the non-Newtonian properties of the blood into consideration, has been studied by Scott et al. [16], Nakamura and Sawada [17], Hogen and Henrikson [18], Srivastava and Saxena [19] and Moayeri and Vali [20].

As some examples of pulsatile flow through stenotic arteries, Back et al. [21] obtained a numerical

1. *Department of Mechanical Engineering, School of Engineering, Shiraz University, Shiraz, I.R. Iran.*
*. *Corresponding Author, Department of Mechanical Engineering, School of Engineering, Shiraz University, Shiraz, I.R. Iran.*

solution to pulsatile flow in the coronary artery of man with double constrictions. The wall was assumed rigid and Navier-Stokes equations, written in terms of vorticity and stream function, were solved through a finite difference method. In that study, a measured flow rate-time relationship for the left coronary was used as the forcing function. O'Brien and Ehrlich [22] used a simple sinusoidal flow and the vorticity-stream function formulation of Navier-Stokes equations to obtain a numerical solution for pulsatile flow in a rigid stenosis. Theodorou and Bellet [23] used a perturbation method along with a finite difference algorithm to obtain an approximate solution for pulsatile flow of a power-law fluid in the rigid stenoses. A cosine function was used for the flowrate-time relationship and the variations of pressure gradient and the wall shearing stress with time were obtained for different values of the power-law index and Reynolds number. Approximate analytical solutions to pulsatile flow in mild stenoses have been reported by Misra and Chakravarty [24], Misra et al. [25] and Cavalcanti [26]. In these, the elastic properties of the wall have been included in the analysis.

It is seen that most experimental and numerical studies of pulsatile flow through stenotic arteries have been performed under the assumption of a simple periodic variation of the inflow with time, i.e., one harmonic. However, from the available data on canine and human arteries, the arterial flux waves are different from a single harmonic pulse and, therefore, for an accurate prediction of pulsatile flow characteristics through stenotic arteries, the actual physiological flow-time variation should be considered.

The main purpose of the present study is to compare the physiological flow characteristics in a stenosis with those obtained under the assumption of a simple harmonic flow. For the physiological flow, the waveform given in [27] for the canine femoral artery (Figure 7) is used. Numerical solutions are obtained under the conditions of laminar flow, Newtonian fluid and axially symmetric rigid stenoses of different severity. Using a non-orthogonal grid, discrete forms of the transformed governing equations are obtained by a control volume formulation and solved for physical velocity components and pressure. For pressure-velocity coupling, SIMPLER algorithm is used. It is concluded that for an accurate analysis of pulsatile flow through stenotic arteries, the actual physiological waveform should be considered for the inflow boundary condition.

GOVERNING EQUATIONS

For axially symmetric flow of incompressible and Newtonian fluids, the non-dimensional mass and linear momentum equations in cylindrical coordinates can be written as:

$$\frac{\partial}{\partial z}(ru) + \frac{\partial}{\partial r}(rv) = 0 \,, \tag{1}$$

$$St\frac{\partial}{\partial t}(ru) + \frac{\partial}{\partial z}(ru^2 - \frac{r}{Re}\frac{\partial u}{\partial z}) + \frac{\partial}{\partial r}(ruv - \frac{r}{Re}\frac{\partial u}{\partial r}) = -r\frac{\partial p}{\partial z} \,, \tag{2}$$

$$St\frac{\partial}{\partial t}(rv) + \frac{\partial}{\partial z}(ruv - \frac{r}{Re}\frac{\partial v}{\partial z}) + \frac{\partial}{\partial r}(rv^2 - \frac{r}{Re}\frac{\partial v}{\partial r}) = -r\frac{\partial p}{\partial r} - \frac{v}{rRe}, \tag{3}$$

in which the dimensionless variables $r^* = r/r_0$, $z^* = z/r_0$, $u^* = u/u_0$, $v^* = v/u_0$, $t^* = t/T$ and $p^* = p/\rho u_0^2$ have been used. $St = \frac{r_0}{u_0 T}$ and $Re = \frac{r_0 u_0}{\nu}$ are the Strouhal and Reynolds numbers, respectively, and asterisks have been dropped for convenience. In the dimensionless parameters, u and v are the velocity components in the z and r directions, respectively, r_0 is the undisturbed arterial radius, T is the period and u_0 is the maximum average velocity over the inlet section. For steady flow, this is the average flow velocity. Considering a general transformation $\xi = \xi(r, z)$ and $\eta = \eta(r, z)$ and using the chain rule of partial differentiation, the governing equations can be written in the following general form:

$$St\frac{\partial a}{\partial t} + \frac{\partial}{\partial \xi}[r(r_\eta u - z_\eta v)\phi - \frac{r}{JRe}(\alpha\frac{\partial \phi}{\partial \xi} - \beta\frac{\partial \phi}{\partial \eta})] + \frac{\partial}{\partial \eta}[r(z_\xi v - r_\xi u)\phi + \frac{r}{JRe}(\beta\frac{\partial \phi}{\partial \xi} - \gamma\frac{\partial \phi}{\partial \eta})] = S_\phi \,, \tag{4}$$

where $J = z_\xi r_\eta - z_\eta r_\xi$, $\alpha = z_\eta^2 + r_\eta^2$, $\beta = z_\xi z_\eta + r_\eta r_\xi$ and $\gamma = z_\xi^2 + r_\xi^2$. Also, the expressions for a, ϕ and S_ϕ for different equations are as described in Table 1.

In the second part of this study (to be reported in a separate paper), deformability of the wall is taken into consideration, for which a new grid is generated at each iteration. For this reason, the simple non-orthogonal transformation $\xi = z$, $\eta = r/r_b(z)$ has been chosen, where $r_b(z)$ represents the geometry of the wall. With this transformation, the metric coefficients, as well as the transformed equations, assume much simpler forms. Also, for the purpose of clustering the grid lines near the wall and in the vicinity of the stenosis throat, appropriate functions have been used.

Table 1. Description of parameters in the transformed governing equations.

Equation	a	ϕ	S_ϕ
(1)	0	1	0
(2)	Jru	u	$-\frac{\partial}{\partial \xi}(rr_\eta p) + \frac{\partial}{\partial \eta}(rr_\xi p)$
(3)	Jrv	v	$\frac{\partial}{\partial \xi}(rz_\eta p) - \frac{\partial}{\partial \eta}(rz_\xi p) + J(p - \frac{\nu}{rRe})$

DISCRETIZATION OF TRANSFORMED EQUATIONS AND SOLUTION PROCEDURE

To obtain the discrete approximation of Equation 4, control volumes in a staggered arrangement are considered. Each equation is integrated over its proper control volume and values of ϕ and its derivatives at control surfaces are approximated in terms of nodal values at surrounding points where the variable ϕ is stored. This results in the following general equation for the momentum equations:

$$\int\int St\frac{\partial}{\partial t}(rJ\phi)d\xi d\eta = A_{0\phi}\phi_0 + \sum_k A_{k\phi}\phi_k + S_\phi \ , \tag{5}$$

in which k stands for the neighboring nodal points at the east, west, north and south of the grid point "O" and A's are finite-difference coefficients combining the effects of convection and diffusion.

In Equation 5, S_ϕ depends on the neighboring nodal values of velocity and pressure. In calculating ϕ_0 at each iteration, S_ϕ is treated as a constant whose value is obtained using the nodal values of u, v and p calculated in the previous iteration.

The time derivative term in Equation 5 is written as:

$$\int\int St(rJ)_0\frac{\partial\phi_0}{\partial t}d\xi d\eta = B_0(\phi_0^{n+1} - \phi_0^n), \tag{6}$$

in which $B_0 = St(rJ\Delta\xi\Delta\eta)_0/\Delta t$ and n represents the time level. The right-hand side of Equation 5 should also be referenced to a time level. This is done by using a linear combination of the values at time levels n and $n+1$, so that Equation 5 is written as:

$$B_0(\phi_0^{n+1} - \phi_0^n) = \theta(A_{0\phi}\phi_0 + \sum_k A_{k\phi}\phi_k + S_\phi)^{n+1} + (1-\theta)(A_{0\phi}\phi_0 + \sum_k A_{k\phi}\phi_k + S_\phi)^n, \tag{7}$$

in which θ is a weighting factor such that: explicit forward-difference scheme is given by θ=0, Euler implicit scheme by θ=1 and Crank-Nicholson scheme by θ=1/2. To ensure stability, the implicit scheme with $0.5< \theta <1$ was used in this study. In fact, numerical experiments on the simple pulsatile flow in a straight tube showed that in addition to the stability, θ also has an effect on the accuracy of the solution such that accuracy decreases as θ increases towards the value of 1.0. No convergence was obtained for $\theta \leq 0.5$ and, therefore, the optimum value of θ=0.65 was obtained and used in all subsequent calculations.

Equation 7 can be written in the following general form, from which ϕ_0^{n+1} can be calculated, where ϕ may be replaced by u or v:

$$A'_{0\phi}\phi_0^{n+1} = \sum_k A_{k\phi}\phi_k^{n+1} + S'_\phi \ . \tag{8}$$

For pressure calculation, SIMPLER method of Patankar [28] is formulated for use in the $(\xi - \eta)$ plane. In SIMPLER method, pressure is calculated through a pressure equation obtained from the continuity equation and velocity components u and v are corrected based on the pressure corrections calculated by a pressure-correction equation. To save space, derivation of these equations is not given here; their general form is the same as Equation 8 with ϕ taking the values of p and Δp, where Δp is the pressure correction term.

Equation 8 shows that the value of a variable ϕ at the node "O" depends on the values of ϕ at the surrounding nodal points E, W, N and S. When Equation 8 is written for the grid points over a constant ξ-section and previously calculated values of ϕ at the sections $\xi \pm \Delta\xi$ are used, a system of linear equations with tridiagonal matrix is obtained, which is then solved by Thomas algorithm. In this way, each equation is independently solved section by section.

Solution is obtained iteratively and the convergence criterion is defined as $\sum|\text{outflow} - \text{inflow}| < \epsilon$, where ϵ is a small numerical value and summation is over all control volumes. Numerical calculations are performed according to the following steps:

1. A first approximation for u, v and p distribution is assumed.
2. Pressure equation is solved.
3. u and v equations are solved.
4. Δp equation is solved and u and v are corrected.
5. Steps 2 to 4 are repeated until the convergence criterion is satisfied.
6. The above calculations are repeated at each time step for several periods and the results obtained for each period are compared to those for the previous period. A periodic solution is obtained only when the variables calculated at different points and at different times over two successive periods become almost identical.

A computer program in FORTRAN was written to perform the numerical calculations. Extensive numerical experiments on the simple pulsatile flow in a straight tube, for which analytical solution is available, were carried out to study the effect of such factors as the dimensionless time increment and the ratio $\Delta r/\Delta z$, using different clustering coefficients. Numerical solutions, using different values of the above parameters, were obtained and compared with the

analytical solution given in the Appendix. As a result, the optimum values of $\Delta t \leq 0.01$ and $0.4 < \Delta r/\Delta z < 2.5$ were obtained and used in all subsequent calculations. For the case of pulsatile flow through stenoses, a 100×11 grid was found to be optimum for obtaining a grid independent solution. Calculations were performed on a Pentium 120 computer. With $\epsilon =$ 5.0E-4, the average number of iterations to satisfy the convergence criterion at each time step was about 2000. Furthermore, the number of periods over which the calculations had to be continued to obtain a completely periodic solution was ranging from 2 to 4, depending on the stenosis severity and the flow waveform.

VALIDATION OF COMPUTATIONAL RESULTS

To check the validity of the numerical results, the following test cases are considered.

Steady Flow Through a Rigid Stenosis

In this case, numerical solutions to steady flow through a stenosis with 56% area reduction are obtained for different values of Reynolds number. The geometry of the stenosis is specified by the following cosine curve:

$$\frac{r}{r_0} = \begin{cases} 1 - \frac{h}{2r_0}[1 + \cos(\frac{\pi z}{z_0})]; & -z_0 \leq z \leq z_0 \\ 1; & |z| > z_0 \end{cases} \quad (9)$$

where $z_0/r_0 = 4$, $h/r_0 = 1/3$ and $L/r_0 = 32$ (Figure 1).

This geometry has also been used by Forrester and Young [3] and Young and Tsai [4] in their experimental studies and by Deshpande et al. [12] in their numerical solution of Navier-Stokes equations, therefore, comparison can be made with previous theoretical and experimental results.

To obtain steady solution, a time marching technique with the following boundary conditions is used. A fully developed laminar velocity profile is considered at the inlet section $I = 1$, while no specified velocity distribution is given at the exit section $I = IN$. At this section, v is obtained by extrapolation, using the v-values calculated at the previous sections. Moreover, at each iteration, using the form of the u-distribution obtained at the section $(IN - 1)$, values of $u(IN)$ are adjusted such that the continuity of flow between the inlet and outlet sections is satisfied [20].

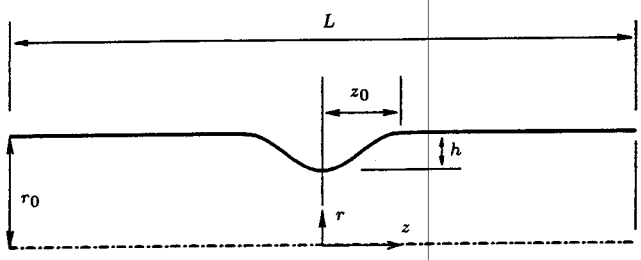

Figure 1. Stenosis geometry used in steady flow analysis.

The variation of dimensionless pressure drop $(\Delta p/\rho u_0^2)$ with Reynolds number is compared with experimental data of Young and Tsai [4] in Figure 2. Considering that initial instability and initial turbulence have been reported by Young and Tsai to occur at $Re = 150$ and $Re = 250$, respectively, Figure 2 demonstrates a good agreement with the experimental measurements in the range of laminar flow conditions.

The separation-reattachment curves from different studies are shown in Figure 3. There is an excellent agreement between the present result and the numerical solution of Deshpande et al. [12]. Also, a good agreement exists between the present

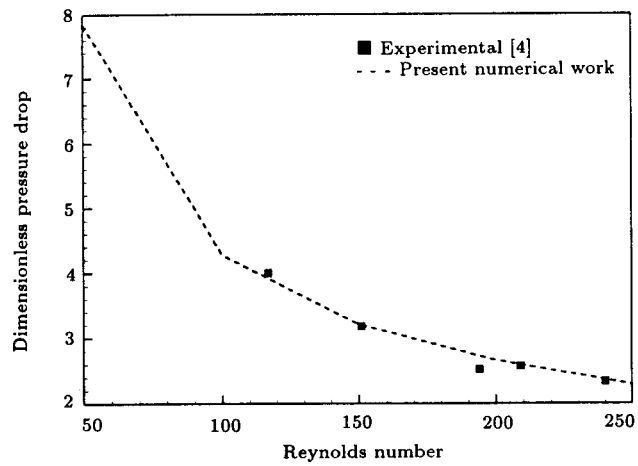

Figure 2. Comparison of pressure drop for steady flow through the stenosis of Figure 1.

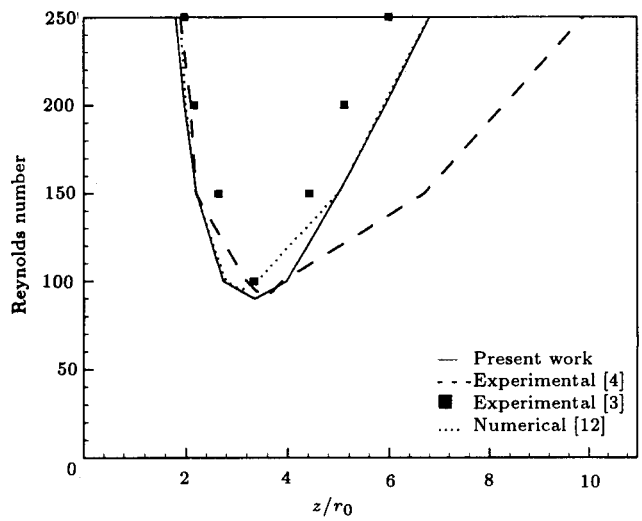

Figure 3. Separation-reattachment curve for steady flow through the stenosis of Figure 1.

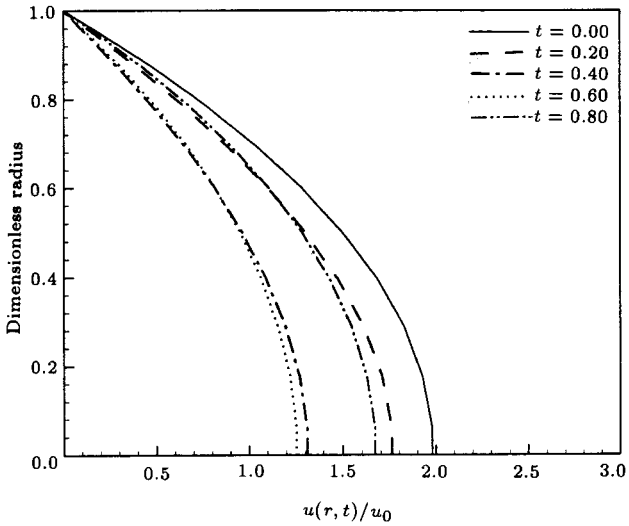

Figure 4. Analytical solution of $u(r,t)$ in a straight tube for the flow given by Equation 10 with $\epsilon_u = 0.2$, $\omega = 2\pi$, $\delta_0 = \pi$, $Re = 100$ and $St = 0.01$.

result and experimental data of Forrester and Young [3]. Apparently, the considerable discrepancy between experimental results of Young and Tsai [4] and those of Forrester and Young indicates a probable mispresentation of the experimental data of Young and Tsai.

Simple Pulsatile Flow in a Straight Rigid Tube

An analytical solution for pulsatile flow in a straight tube is presented in the Appendix. According to that solution, given the mean velocity for a simple pulsatile flow in the form:

$$\bar{u}(t) = 1 - \epsilon_u[1 + cos(\omega t + \delta_0)], \qquad (10)$$

the pressure gradient $-\frac{\partial p(t)}{\partial z}$ and velocity $u(r,t)$ can be obtained. To validate the numerical results, the waveform of $-\frac{\partial p(t)}{\partial z}$ obtained by analytical and numerical solutions are compared in this test case. For this purpose, the input function (Equation 10) with ϵ_u=0.2, $\omega = 2\pi$ and $\delta_0 = \pi$ was first used to obtain analytical solutions for $-\frac{\partial p(t)}{\partial z}$ and $u(r,t)$. Then, the analytical results of $u(r,t)$ were used as the inlet boundary condition to obtain a numerical solution. The analytical solution of $u(r,t)$ for the case of Re = 100 and $St = 0.01$ is shown in Figure 4. Analytical and numerical results for dp/dz are compared in Figure 5, rendering an excellent agreement.

Harmonically Oscillating Flow Through a Stenosis

Young and Tsai [7] have measured the pressure drop across a stenosis with 56% area reduction for an oscillating flow characterized by $\bar{u}(t) = \cos(\omega t)$ and for a Reynolds number of 1830, based on the diameter of

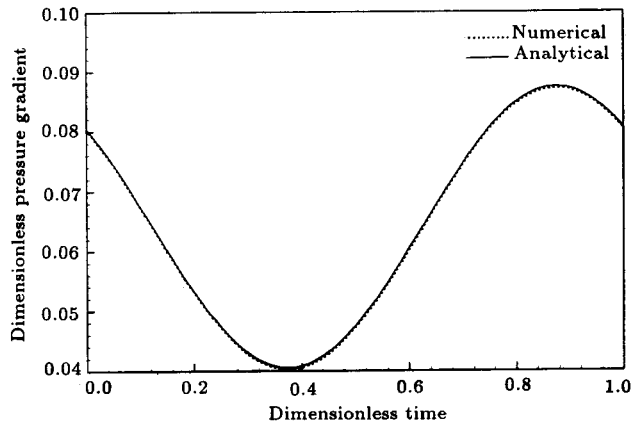

Figure 5. Comparison of analytical and numerical solution of dp/dz for the flow of Figure 4.

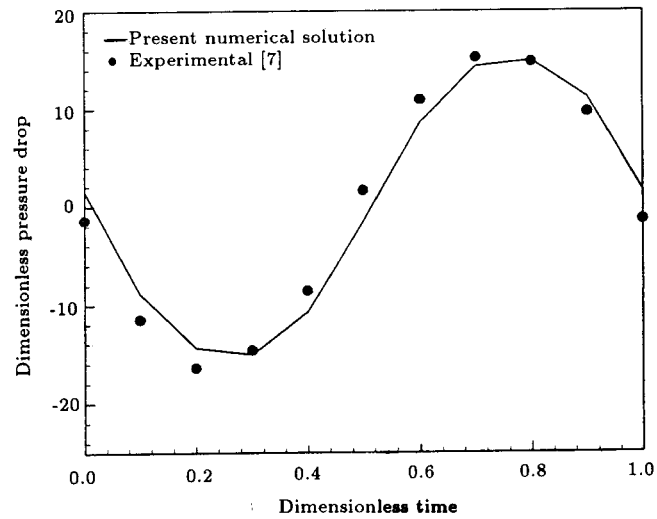

Figure 6. Comparison of dimensionless pressure drop through a stenosis for a harmonically oscillating flow, $h/r_0 = 0.333$, $Re = 915$ and $St = 0.075$.

unconstricted region. The geometry of the stenosis is specified by Equation 9, as shown in Figure 1. In this test case, the above experimental conditions are used to obtain a numerical solution for the same flow with Re = 915 and $St = 0.075$. The waveform for dimensionless pressure drop obtained from the numerical solution is compared with the waveform measured by Young and Tsai in Figure 6. It is seen that the agreement is generally good except for a slight shift in phase which may be due to uncertainities in the measurements.

PHYSIOLOGICAL FLOW THROUGH STENOSES

In this section, numerical solution to a physiological flow through stenoses of different area reduction is presented. The geometry of stenoses is given by Equation 9 (Figure 1), with $z_0/r_0 = 3, L/r_0 = 11$ and

$h/r_0 = 0.125$, 0.250 and 0.375. The physiological flow is specified by the waveform given by Daly [27] for the mean velocity $\bar{u}(t)$ in the canine femoral artery, as shown in Figure 7, for which $Re = 391.2$ and $St = 0.004544$ can be calculated. Using the waveform of Figure 7, analytical solutions for $u(r,t)$ and $\frac{\partial p(t)}{\partial z}$ for flow in a straight tube are obtained (see the Appendix), which are shown in Figures 8 and 9, respectively. The $u(r,t)$ given in Figure 8 is then used as the boundary condition at the inlet section for the numerical solution of the physiological flow through the stenoses. As a further validation of the numerical results, this boundary condition was also used to obtain a numerical solution for $\frac{\partial p(t)}{\partial z}$ in a straight tube, which is compared with the analytical results in Figure 9.

Enormous information is obtained by numerical solution of pulsatile flow through stenoses, so that a decision should be made on the types of information (and also the form of presentation) to be included in a paper to illustrate the significant behavior of the flow. Therefore, only a limited amount of results, specially at instances marked by A, B, C and D in Figure 7, are presented here.

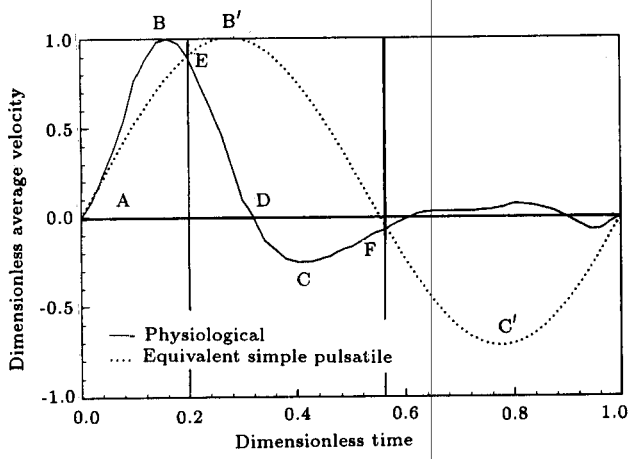

Figure 7. Time variation of the mean velocity for the physiological flow [27] and for an equivalent simple pulsatile flow (see Sec. 6).

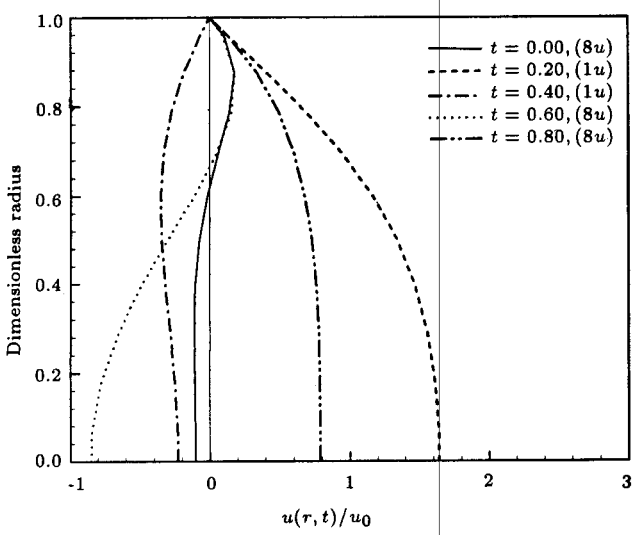

Figure 8. Analytical solution of $u(r,t)$ for the physiological flow of Figure 7 in a straight tube.

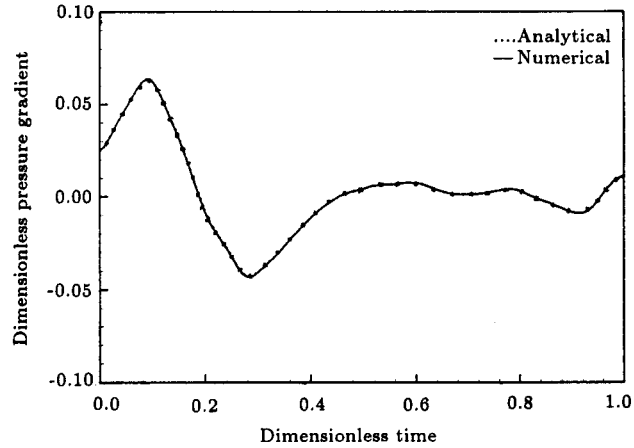

Figure 9. Pressure gradient for the physiological flow of Figure 7 in a straight tube (analytical and numerical results are exactly the same).

The waveforms of pressure drop for physiological flow through stenoses of different severity are illustrated in Figure 10. According to this figure, there is no significant difference in the waveforms for different stenoses at diastolic phase after the maximum backflow, corresponding to the point C in Figure 7. However, the pressure drop corresponding to the systolic peak increases with increasing stenosis severity. Also, note that there is a shift in phase between $\bar{u}(t)$ and $\Delta p/\rho u_0^2$.

The dimensionless wall shear stress for physiological flow through the stenoses and at four instances A, B, C and D are demonstrated in Figure 11, in which different scales have been used for τ at different

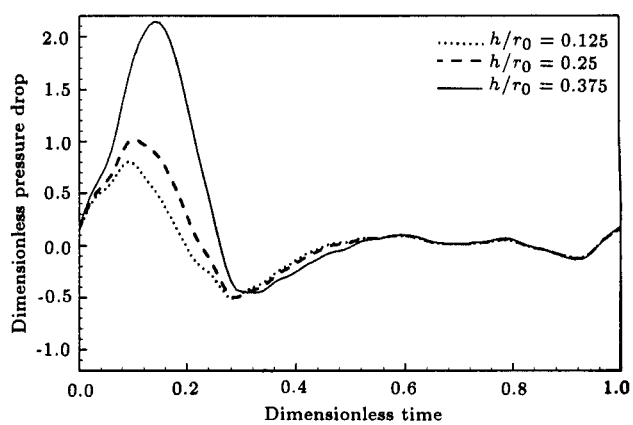

Figure 10. The waveforms of pressure drop for the physiological flow.

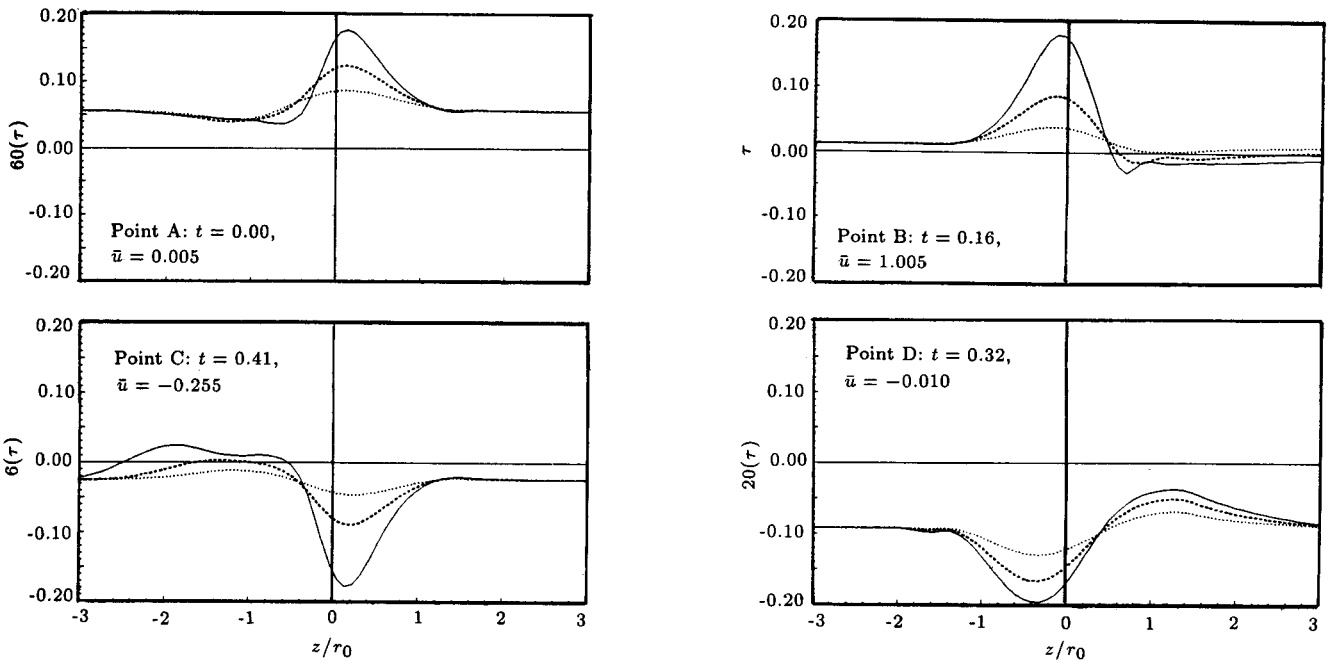

Figure 11. Wall shear stress, $Re = 391.2$, $St = 0.004544$, (_____)$h/r_0 = 0.375$, (– – – –)$h/r_0 = 0.25$, (.....)$h/r_0 = 0.125$.

instances. Figure 11 reveals that: a) No separated flow exists for the stenosis of $h/r_0 = 0.125$ at all four instances considered. b) For small values of q, with either forward or backward flow next to the boundary, such as points A and D, separation does not occur in any of the three stenoses. c) Maximum absolute value of the wall shear stress increases with increasing stenosis severity. d) The location of the maximum absolute wall shear stress shifts from one side of the throat to the other side as q changes from zero (points A and D) towards its peak (points B and C).

COMPARISON OF NUMERICAL SOLUTIONS FOR PHYSIOLOGICAL AND SIMPLE PULSATILE FLOW

In this section, the behavior of physiological flow through a stenosis is compared with that of an equivalent simple pulsatile flow. Equivalent simple pulsatile flow is considered as a flow specified by Equation 10, with $\bar{u}(0) = 0$, having the same stroke volume as the physiological flow. Applying the condition $\bar{u}(0) = 0$ to Equation 10, $\delta_0 = cos^{-1}(\frac{1-\epsilon_u}{\epsilon_u})$ is obtained. Then, integrating the waveform of the physiological flow given in Figure 7 and also Equation 10 over one period, 0.142 and (1-ϵ_u) are obtained, respectively, so that the ϵ_u-value of the equivalent simple pulsatile flow is 0.858. The waveform for the equivalent flow is also shown in Figure 7.

The boundary condition $u(r,t)$ at the inlet section required for obtaining the numerical solution of the equivalent flow is found through the analytical solution of this flow in a straight tube, as discussed in the Appendix. Numerical solutions for the physiological and equivalent simple pulsatile flow are obtained only for the stenosis of $h/r_0 = 0.375$. Different approaches can be considered for comparing the behavior of these flows as fluid passes through the stenosis. In one approach, the results can be compared at the same instances of time. Another approach is to compare the results at three points corresponding to conditions of initial zero, peak forward and peak backward flow rates on each waveform, i.e., at points A, (B,B′) and (C,C′) in Figure 7. Nevertheless in another approach, the results are compared at the points A, E and F where two flows have equal flow rates at the same time instances. Apparently, using different approaches, different conclusions may be drawn from the comparisons. In the following, the comparison of results based on the second approach is first presented. Then, to show the difference, results are also compared at the points E and F and at the instance when physiological flow rate takes on its first zero during diastolic phase, i.e., point D in Figure 7.

Axial velocity distribution at some different sections and the wall shear stress for the physiological and the equivalent simple pulsatile flow at points A, (B,B′) and (C,C′) are shown in Figure 12. In this figure, shear stress is measured vertically from the stenosis boundary. Note that, to show the differences more clearly, different scales have been chosen for each variables u and τ at the points A, B and C.

As seen, at the point A ($t = 0$), where both flow rates are almost zero, the trend of variation of shear stress along the flow is almost the same for both flows except that the magnitude of shear stress for the simple

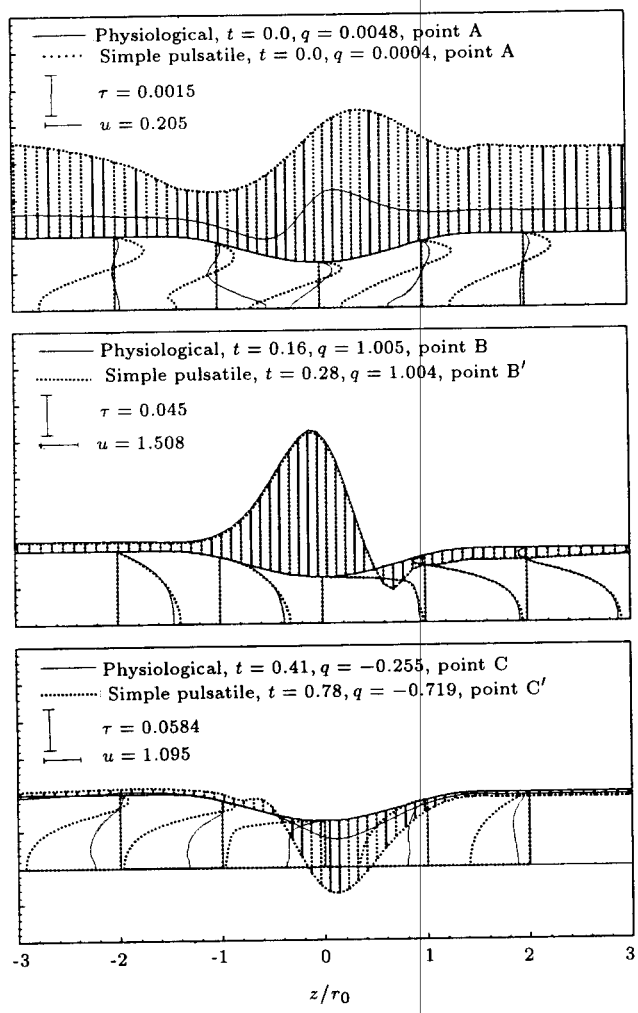

Figure 12. Axial velocity distribution at different sections and wall shear stress for the physiological and equivalent simple pulsatile flow at points A, (B,B′) and (C,C′), $h/r_0 = 0.375$, $Re = 391.2$ and $St = 0.004544$.

flow is much larger than that for the physiological flow. This is because there is a forward flow next to the boundary in both cases, however, the forward flow rate is greater in the simple flow. This can be explained with the help of Figure 16. There is a significant forward flow near the boundary and almost equal backward flow in the central portion in the simple flow, resulting in a negligible flow of q =0.0004. On the other hand, Figure 16 indicates that there is no backward flow in the central portion in the physiological flow and therefore, only a small amount of $q = 0.0048$ takes place next to the boundary.

Figure 12 demonstrates that there is no significant difference between shear stress distributions at the points (B,B′) where both flows are at their peak. Under this condition, there is a comparable separation region at the downstream vicinity of the throat for both flows. At the points (C,C′), where both flows occur in reverse direction, the magnitude of shear stress for the simple flow is much larger. Furthermore, there is a small separation region at upstream of the throat for the physiological flow while the separation region in the simple flow is much longer. This is due to the fact that at point C′, the magnitude of flow rate for the equivalent simple flow is almost three times as large as that for the physiological flow at point C.

Figure 13 depicts the comparison of the wall shear stress and u-velocity distributions of the two flows at the instance shown by point D in Figure 7. According to this figure, there is a reverse flow near the boundary and a slightly smaller forward flow in the central region for the physiological flow, resulting in an overall reverse flow of q = -0.0104 with no separation region. In spite of that, the whole simple flow occurs in the positive direction with a long separation region downstream of the throat. Figure 14 indicates that the behavior of

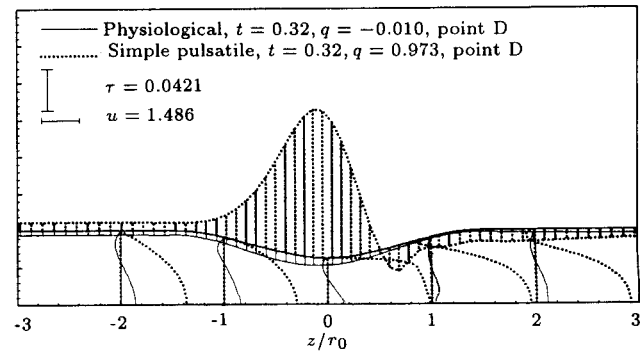

Figure 13. Comparison of u-velocity distribution and wall shear stress for the two flows at the instance D of Figure 7.

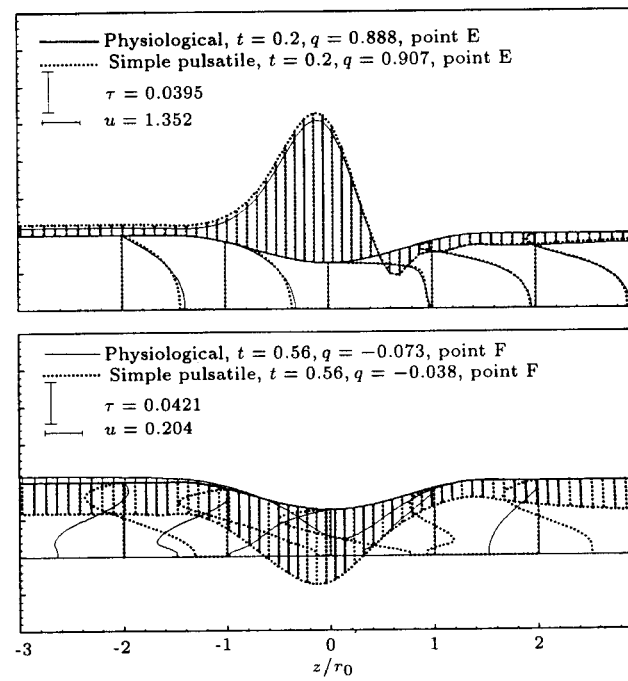

Figure 14. Comparison of u-velocity distribution and wall shear stress for the two flows at the instances E and F of Figure 7.

the two flows is almost the same at $t = 0.2$ (point E) where flow rates are also almost the same. However, this situation does not exist at $t = 0.56$ (point F) where both flow rates are again almost the same. Note that the comparison has not been made exactly at the point in question because the results of calculations have been stored only at each 0.02 dimensionless-time intervals. That is why there is a slight difference in q for the two flows at the instances of time marked by points E and F, for example.

Variation with time of the wall shear stress at different sections of the two flows can also be compared. This is done only for the section $z = 0$, which is shown in Figure 15. The waveform of $\bar{u}(t)$ for the two flows are also presented in this figure which indicates that the waveform of the wall shear stress at section $z = 0$ is almost the same as that of $\bar{u}(t)$ for each flow and only the numerical values of τ *and* $\bar{u}(t)$ are different. However, the numerical results (not shown here) indicate that this is not the case for any other section.

Streamlines of the two flows at point A are compared in Figure 16. The physiological flow has 2 stagnation points on the center line and 2 stagnation rings, forming 4 vortex rings, with a small amount of forward flow next to the boundary. On the other hand, the simple pulsatile flow has only one stagnation ring with no stagnation point on the center line. Therefore, simple flow consists of 2 vortex rings of

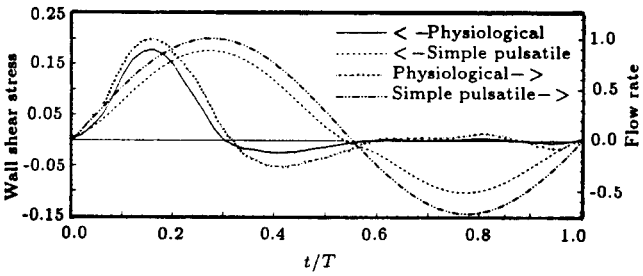

Figure 15. Time variation of the wall shear stress for the physiological and equivalent simple pulsatile flow at $z = 0$.

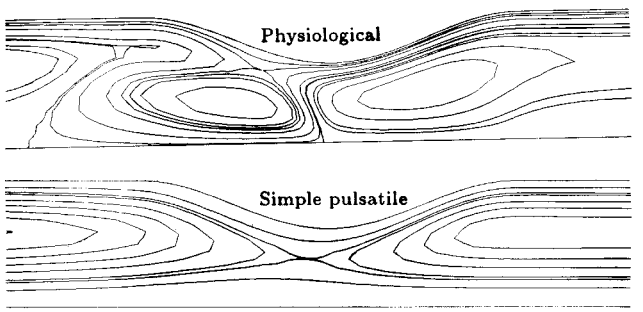

Figure 16. Comparison of streamlines for the physiological and simple pulsatile flow at the point A of Figure 7.

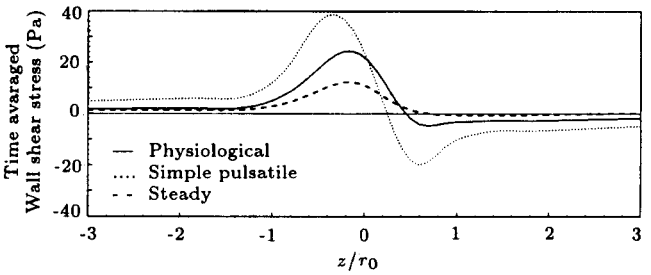

Figure 17. Time average of the wall shear stress, $h/r_0 = 0.375$.

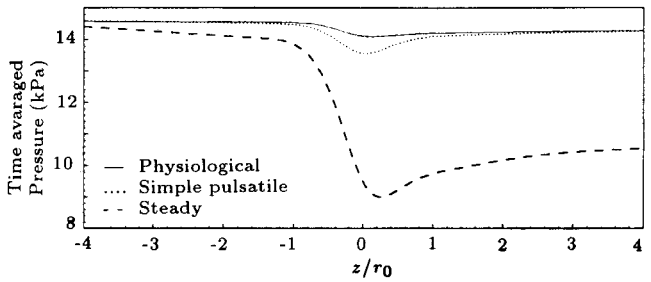

Figure 18. Time average of center line pressure, $h/r_0 = 0.375$.

opposite directions at the upstream and downstream of the throat, a relatively large forward flow next to the boundary and an almost equal backward flow in the central region. According to Figure 16, the behavior of the two flows is completely different at point A, while Figure 12 indicates a similar trend for the wall shear stress at that point.

Although the time average of flow variables is not indicative of the pulsatile flow behavior, the time averaged wall shear stress and center line pressure for the physiological, equivalent simple pulsatile and an equivalent steady flow are compared in Figures 17 and 18, respectively. Figure 17 illustrates that the largest range of variation (maximum minus minimum) of the time averaged wall shear stress occurs for the simple pulsatile flow and the smallest range for the steady flow. Figure 18 indicates that based on the time average of the center line pressure, the pressure drop for the physiological and simple pulsatile flow is the same and much smaller than that of the steady flow. Note that the Reynolds number for the equivalent steady flow is 55.55; that is why Figure 17 indicates that there is no separated region for the steady flow.

SUMMARY AND CONCLUSION

Most experimental and numerical studies of pulsatile flow through stenotic arteries have been performed assuming a simple harmonic pulse as the inflow boundary condition. In this paper, numerical solutions to a physiological flow and a simple harmonic flow of the same stroke volume through a stenosis with 61% area

reduction have been obtained and some of the results have been compared. Comparison mostly includes the wall shear stress distribution and axial velocity profile at different sections, which is made at some time instances.

Different approaches have been used to compare the results. In one approach, comparison is made at some time instances when both flows have zero, peak forward and peak backward flow rates (Figure 12). This indicates that the behavior of the two flows is similar only when they are at their peak forward flow, which occurs at different time instances. In the second approach, comparison is made at a common time instance (Figure 13, point D) when the flow rates are different. This shows two completely different behaviors for the two flows. In the third approach, comparison is made at the instances when both flows have equal flow rates (Figure 12, point A, Figure 14, points E and F). This demonstrates a similar behavior only at point E (Figure 7) where the simple flow approaches its systolic peak but the physiological flow is at the beginning of its diastolic phase.

Comparison of the time variation of the wall shear stress at different sections indicates that the waveform of τ is almost the same as that of $\bar{u}(t)$ at the throat of the stenosis and this is the case only at this section. Comparison of the time average of the wall shear stress distribution illustrate a larger variation of τ for the simple flow (Figure 17). Also, comparison of the time average of center line pressure (Figure 18) shows that the pressure drop of the two flows are equal and much smaller than that of an equivalent steady flow.

Comparison of streamlines of the two flows has also been made at different time instances, although only at $t = 0$ has been presented (Figure 16). This, too, indicates that the relatively close similarity of the flow behavior exists in some instances.

The present analysis shows that although the behaviors of the two flows are almost similar in some instances, they should be considered as two flows with completely different behaviors. Therefore, for an accurate analysis of pulsatile flow through stenotic arteries, the actual physiological waveform should be considered as the inflow boundary condition.

REFERENCES

1. Nerem, R.M. "Vascular fluid mechanics, the arterial wall and atherosclerosis", *J. Biomech. Eng., Trans. ASME*, **114**, pp 274-282 (1992).
2. Giddens, D.P., Zarins, C.K. and Glagov, S. "The role of fluid mechanics in the localization and detection of atherosclerosis", *J. Biomech. Eng., Trans. ASME*, **115**, pp 588-594 (1993).
3. Forrester, J.H. and Young, D.F. "Flow through a converging-diverging tube and its implications in occlusive vascular disease", *J. Biomechanics*, **3**, pp 307-316 (1970).
4. Young, D.F. and Tsai, F.Y. "Flow characteristics in models of arterial stenoses-I. Steady flow", *J. Biomechanics*, **6**, pp 395-410 (1973).
5. Ahmed, S.A. and Giddens, D.P. "Velocity measurement in steady flow through axisymmetric stenoses at moderate Reynolds numbers", *J. Biomechanics*, **16**, pp 505-516 (1983).
6. Cavalcanti, S., Bolelli, P. and Belardinelli, E. "Pressure drops through arterial stenosis models in steady flow condition", *J. Biomech. Eng., Trans. ASME*, **114**, pp 416-418 (1992).
7. Young, D.F. and Tsai, F.Y. "Flow characteristics in models of arterial stenoses-II. Unsteady flow", *J. Biomechanics*, **6**, pp 547-559 (1973).
8. Siouffi, M., Pelissier, R., Farahifar, D. and Rieu, R. "The effect of unsteadiness on the flow through stenoses and bifurcations", *J. Biomechanics*, **17**, pp 299-315 (1984).
9. Rabinovitz, R., Degani, D. and Gutfinger, C. "An experimental study of pressure losses in pulsatile flows through rigid and pulsating stenosis", *J. Biomech. Eng., Trans. ASME*, **106**, pp 309-314 (1984).
10. Lieber, B.B. and Giddens, D.P. "Apparent stresses in disturbed pulsatile flows", *J. Biomechanics*, **21**, pp 287-298 (1988).
11. Rooz, E., Young, D.F. and Rogge, T.R. "A finite-element simulation of pulsatile flow in flexible obstructed tubes", *J. Biomech. Eng., Trans. ASME*, **104**, pp 119-124 (1982).
12. Deshpande, M.D., Giddens, D.P. and Mabon, R.F. "Steady laminar flow through modeled vascular stenoses", *J. Biomechanics*, **9**, pp 165-174 (1976).
13. Fukushima, T., Azuma, T. and Matsuzawa, T. "Numerical analysis of blood flow in the vertebral artery", *J. Biomech. Eng., Trans. ASME*, **104**, pp 143-147 (1982).
14. Lee, T.S. "Numerical studies of fluid flow through tubes with double constrictions", *Int. J. for Numerical Methods in Fluids.*, **11**, pp 1113-1126 (1990).
15. Siegel, J.M., Markou, C.P., Ku, D.N. and Hanson, S.R. "A scaling law for wall shear rate through an arterial stenosis", *J. Biomech. Eng., Trans. ASME*, **116**, pp 446-451 (1994).
16. Scott, P.S., Misra, F. and Vlachopoulos, J. "A finite element analysis of laminar viscoplastic flows in systems with flow separation", *Proceeding of the Fifth Int. Conf. on Num. Methods in Laminar and Turbulent Flow* (1987).
17. Nakamura, M. and Sawada, T. "Numerical study on the flow of a non-Newtonian fluid through an axisymmetric stenosis", *J. Biomech. Eng., Trans. ASME*, **110**, pp 137-143 (1988).
18. Hogen, H.A. and Henriksen, M. "An evaluation of a micropolar model for blood flow through an idealized stenosis", *J. Biomechanics*, **22**, pp 211-218 (1989).

19. Srivastava, V.P. and Saxena, M. "Two-layered model of Casson fluid flow through stenotic blood vessels: applications to the cardiovascular system", *J. Biomechanics*, **27**, pp 921-928 (1994).
20. Moayeri, M.S. and Vali, A. "Effects of non-Newtonian properties of blood on flow characteristics through a stenosis", *Iranian J. of Science and Technology*, **20**, pp 25-43 (1996).
21. Back, L.D., Radbill, J.R. and Crawford, D.W. "Analysis of pulsatile, viscous blood flow through diseased coronary arteries of man", *J. Biomechanics*, **10**, pp 339-353 (1977).
22. O'Brien, V. and Ehrlich, L.W. "Simple pulsatile flow in an artery with a constriction", *J. Biomechanics*, **18**, pp 117-127 (1985).
23. Theodorou, G. and Bellet, D. "Laminar flows of a non-Newtonian fluid in mild stenosis", *Computer Methods in Applied Mechanics and Engineering*, **54**, pp 111-123 (1986).
24. Misra, J.C. and Chakravarty, S. "Flow in arteries in the presence of stenosis", *J. Biomechanics*, **19**, pp 907-918 (1986).
25. Misra, J.C., Patra, M.K. and Misra, S.C. "A non-Newtonian model for blood flow through arteries under stenotic conditions", *J. Biomechanics*, **26**, pp 1129-1141 (1993).
26. Cavalcanti, S. "Hemodynamics of an artery with mild stenosis", *J. Biomechanics*, **28**, pp 387-399 (1995).
27. Daly, B.J. "A numerical study of pulsatile flow through stenosed canine femoral arteries", *J. Biomechanics*, **9**, pp 465-475 (1976).
28. Patankar, S.V., *Numerical Heat Transfer and Fluid Flow*, Hemisphere Publishing Co., Washington, D.C., USA (1980).

APENDIX

The dimensionless equation for pulsatile flow in a straight tube can be written as:

$$St\frac{\partial u}{\partial t} - \frac{1}{rRe}\frac{\partial}{\partial r}(r\frac{\partial u}{\partial r}) = -\frac{\partial p}{\partial z} . \tag{A1}$$

Solution to homogeneous form of Equation A1 can be written in terms of its eigenfunctions as:

$$u(r,t) = \sum_{n=1}^{\infty} a_n(t) J_0(\lambda_n r) , \tag{A2}$$

where J_0 is the Bessel function of the first kind and the eigenvalues λ_n's are obtained using the boundary condition $u(1,t) = 0$. Substitution of Equation A2 into A1 results in:

$$\sum_{n=1}^{\infty}(St\frac{da_n}{dt} + \frac{\lambda_n^2}{Re}a_n)J_0(\lambda_n r) = -\frac{\partial p}{\partial z} . \tag{A3}$$

For a simple harmonic flow, $\frac{\partial p}{\partial z}$ can be written as:

$$-\frac{\partial p}{\partial z} = \bar{\Phi} + \tilde{\Phi}\sin(\omega t + \delta) , \tag{A4}$$

so that Equation A3 is written as:

$$\sum_{n=1}^{\infty}(St\frac{da_n}{dt} + \frac{\lambda_n^2}{Re}a_n)J_0(\lambda_n r) = \bar{\Phi} + \tilde{\Phi}\sin(\omega t + \delta) . \tag{A5}$$

When Equation A5 is multiplied by $rJ_0(\lambda_n r)dr$ and integrated from 0 to 1, the following equation for $a_n(t)$ is obtained:

$$St\frac{da_n}{dt} + \frac{\lambda_n^2}{Re}a_n = \frac{2[\bar{\Phi} + \tilde{\Phi}\sin(\omega t + \delta)]}{\lambda_n J_1(\lambda_n)} . \tag{A6}$$

Now, assuming $a_n(t) = C_n + A_n\sin(\omega t) + B_n\cos(\omega t)$, it can be shown that:

$$C_n = \frac{2Re\bar{\Phi}}{\lambda_n^3 J_1(\lambda_n)} , \tag{A7}$$

$$A_n = 2Re\tilde{\Phi}(\omega ReSt\sin\delta + \lambda_n^2\cos\delta)/D_n , \tag{A8}$$

$$B_n = 2Re\tilde{\Phi}(\lambda_n^2\sin\delta - \omega ReSt\cos\delta)/D_n , \tag{A9}$$

in which,

$$D_n = \lambda_n J_1(\lambda_n)[(\omega ReSt)^2 + \lambda_n^4] .$$

Therefore, for a known pressure gradient $\frac{\partial p}{\partial z}$ as in Equation A4 and given values of Re and St, $a_n(t)$ can be calculated using Equations A7 to A9 and then is substituted into Equation A2 to obtain $u(r,t)$.

Likewise, for a simple harmonic flow, the dimentionless flow rate can be written as:

$$q(t) = \bar{u}(t) = 1 - \varepsilon[1 + \cos(\omega t + \delta_0)] . \tag{A10}$$

Therefore,

$$1 - \varepsilon[1 + \cos(\omega t + \delta_0)] = 2\int_0^1 ru(r,t)dr .$$

Substitution for $u(r,t)$ from Equation A2 results in the following equation:

$$1 - \varepsilon - \varepsilon\cos\omega t\ \cos\delta_0 + \varepsilon\sin\omega t\ \sin\delta_0$$

$$= \sum_{n=1}^{\infty}\frac{2J_1(\lambda_n)}{\lambda_n}(C_n + A_n\sin\omega t + B_n\cos\omega t). \tag{A11}$$

Substituting for C_n, A_n and B_n from Equations A7 to A9 and equating the coefficient of like terms at two sides of Equation A11, it is obtained that:

$$\bar{\Phi} = \frac{1-\varepsilon}{4ReS_1}, \tag{A12}$$

$$\delta = \tan^{-1}\frac{\omega ReStS_3\tan\delta_0 - S_2}{\omega ReStS_3 + S_2\tan\delta_0}, \tag{A13}$$

$$\tilde{\Phi} = \frac{\varepsilon\sin\delta_0}{4\ Re(\omega ReStS_3\sin\delta + S_2\cos\delta)}, \tag{A14}$$

in which,

$$S_1 = \sum_{n=1}^{\infty}\frac{1}{\lambda_n^4} = \frac{1}{8}\ , \tag{A15}$$

$$S_2 = \sum_{n=1}^{\infty}\frac{1}{(\omega ReSt)^2 + \lambda_n^4}, \tag{A16}$$

$$S_3 = \sum_{n=1}^{\infty}\frac{1}{\lambda_n^2[(\omega ReSt)^2 + \lambda_n^4]}. \tag{A17}$$

Therefore, for a known flow rate as in Equation A10 and given values of Re and St, $\bar{\Phi}$ and $\tilde{\Phi}$ and δ can be calculated from Equations A12 to A14, that is, $\frac{\partial p}{\partial z}$ is obtained.

Any waveform of a physiological flow, either $\bar{u}(t)$ or $\frac{\partial p(t)}{\partial z}$, can be expanded in terms of Fourier series. For example, when the waveform of $\bar{u}(t)$ is known, it can be written as:

$$\bar{u}(t) = A_1 + \sum_{j=1}^{N}[A_{j+1}\sin(2j\pi t) + A_{j+N+1}\cos(2j\pi t), \tag{A18}$$

where the coefficients A_1 to A_{2N+1} can be obtained from the given waveform using the method of least square. For this case, Equations A2 and A4 are, respectively, written as:

$$u(r,t) = \sum_{j=1}^{N+1}\sum_{n=1}^{\infty}a_{j,n}(t)J_0(\lambda_n r), \tag{A19}$$

$$-\frac{\partial p}{\partial z} = B_1 + \sum_{j=1}^{N}[B_{j+1}\sin(2j\pi t) + B_{j+N+1}\cos(2j\pi t)], \tag{A20}$$

so that:

$$St\frac{\partial u_1}{\partial t} - \frac{1}{r\ Re}\frac{\partial}{\partial r}(r\frac{\partial u_1}{\partial r}) = B_1$$

$$St\frac{\partial u_{j+1}}{\partial t} - \frac{1}{r\ Re}\frac{\partial}{\partial r}(r\frac{\partial uj+1}{\partial r})$$

$$= B_{j+1}\sin(2j\pi t) + B_{j+N+1}\cos(2j\pi t);$$

$$j = 1, 2, ..., N, \tag{A21}$$

where the coefficients B's can be obtained in terms of the known values of A's using the same method as used for Equation A5. The results are as the following:

$$B_1 = \frac{8A_1}{Re}$$

$$B_{j+1} = \frac{S_2A_{j+1} - S_3C_jA_{j+N+1}}{4Re(S_2^2 + S_3^2C_j^2)};\quad j = 1, 2, ...N$$

$$B_{j+N+1} = \frac{S_2A_{j+N+1} + S_3C_jA_{j+1}}{4Re(S_2^2 + S_3^2C_j^2)};\quad j = 1, 2, ...N,$$

in which $C_j = 2j\pi ReSt$ and S_2 and S_3 are given by Equations A16 and A17, respectively. Then, $u_(r,t)$ is obtained from Equation A19 in which:

$$a_{1,n}(t) = \frac{2B_1Re}{\lambda_n^3J_1(\lambda_n)},$$

$$a_{j+1,n}(t) = \frac{2Re}{\lambda_nJ_1(\lambda_n)(C_j^2 + \lambda_n^4)}$$

$$[(C_jB_{j+N+1} + \lambda_n^2B_{j+1})\sin(2j\pi t)$$

$$+ (\lambda_n^2B_{j+N+1} - C_jB_{j+1})\cos(2j\pi t)];$$

$$j = 1, 2, ...N\ .$$